Journal of Materials and Environmental Sciences
ISSN : 2028-2508

JMES, 2017 Volume 8, Issue 6, Page 1935-1947

http://www.jmaterenvironsci.com/

Electrochemical and theoretical studies of adsorption and corrosion inhibition of 1-methyl-4-methylsulfanyl- 1H-pyrazolo[3,4-d]pyrimidine on mild steel in acidic solution

J. Bouhoud[1], M. El Fal[2,3],Y. Ramli[2]*, S. Echihi[1,4], A. Zarrouk[5], M. Tabyaoui[1], A. Guenbour[1], A. Bellaouchou[1], E.M. Essassi[3]

1.Laboratory of Materials, Nanotechnology and Environment, Faculty of Science, University of Mohamed-V Av. Ibn Battouta, BP 1014 Rabat, Morocco.

2. Medicinal Chemistry Laboratory, Faculty of Medicine and Pharmacy, Mohammed V University, Rabat, Morocco

3. Laboratoire de Chimie Organique Hétérocyclique URAC 21, Pôle de Compétence Pharmacochimie, Faculté des Sciences, Université Mohammed V, Rabat, Morocco.

4. Laboratory of Water and Environment, Faculty of Sciences of El jadida, BP 20, 24000 El jadida, Morocco.

5. LCAE-URAC 18, Faculty of Science, First Mohammed University, PO Box 717, 60 000 Oujda, Morocco.

Received 22 Feb 2016,
Revised 25 Fab2017,
Accepted 05 Mar 2017

Keywords

- ✓ Mild Steel;
- ✓ Corrosion;
- ✓ Inhibition;
- ✓ Pyrazolo[3,4-d]pyrimidine derivative
- ✓ DFT;

Y. Ramli
yramli76@yahoo.fr
+212670515279

Abstract

The inhibition effect of 1-methyl-4-methylsulfanyl-1H-pyrazolo[3,4-d]pyrimidine (MMPP) on the corrosion of mild steel in 1.0 M HCl solution using electrochemical techniques (electrochemical impedance spectroscopy and potentiodynamic polarization). The results show that synthesized pyrimidine derivative is excellent inhibitor even with very low concentration, and the adsorption on mild steel surface obeys Langmuir adsorption isotherm. The potentiodynamic polarization results indicated that the studied inhibitor act as mixed type. Adsorption of used inhibitor led to a reduction in the double layer capacitance and an increase in the charge transfer resistance. Thermodynamic and activation parameters were discussed. Calculated ΔG°_{ads} value indicated that the adsorption mechanism of the prepared pyrimidine derivative on mild steel in 1.0 M HCl solution is a chemical adsorption. Quantum chemical calculations were used to correlate the inhibition ability of MMPP with its electronic structural parameters.

1. Introduction

The control of mild steel corrosion has become an issue of significant concern for materials technologists and corrosion scientists. Despite the fact that mild steel finds wide range of technological applications such as petroleum production and refining, chemical processing, marine applications and construction [1-7], its poor corrosion resistance especially in acid solutions [8,9] curtails its utility. Acid solutions are widely used as descaling, pickling and cleaning agents in industries, and thus generate corrosive effects on mild steel and other materials made of iron [10,11]. Among the various methods used to control the corrosion process [12], application of inhibitors is the most practical and efficient way to achieve this objective.

Organic compounds, especially those containing polar functions with oxygen, nitrogen and/or sulfur in a conjugated system are usually employed as inhibitors against the corrosion of metals in aggressive environments [13-33]. They function by adsorption on metal surfaces, and thus form protective layers that hinder the corrosion process. In terms of adsorption strength of inhibitors, certain factors are of significant consideration, including: the nature and surface charge of the metal, composition of the electrolyte and the structure of the inhibitor.

Density functional theory (DFT) has grown to be a useful theoretical method to interpret experimental results, enabling one to obtain structural parameters for even huge complex molecules, and it can explains the hard and soft acid base (HSAB) behavior of organic molecules, i.e., DFT connects some traditional empirical concepts with quantum mechanical interpretations [34,35]. Therefore, DFT is very powerful technique to probe the

inhibitor/surface interaction and to analyze experimental data. These are the reasons why we selected both electrochemical and DFT methods to evaluate the efficiency of 1-methyl-4-methylsulfanyl-1H-pyrazolo[3,4-d]pyrimidine (MMPP).The objective of this study is to investigate the efficiency of novel pyrimidine derivative as corrosion inhibitor of mild steel in 1.0 M HCl. The inhibition efficiency of this compound was determined by using potentiodynamic polarization and electrochemical impedance spectroscopy. The thermodynamic parameters and activation of inhibitor were studied.

2. Experimental details

2.1. Materials

The material used in this study is a mild steel with a chemical composition(in wt%) 0.37% C, 0.23%Si, 0.016 S%, 0,68 Mn%, 0.16 Cu%, 0.077Cr%, 0.011Ti%, 0,052Ni%, 0.009 Co% and the remainder iron (Fe). The steel samples were pre-treated prior to the experiments by grinding with emery paper sic (230, 400, 600, 1200 and 1500); rinsed with distilled water, degreased in acetone, washed again with bidistilled water and then dried at room temperature before use.

2.2. Solutions

The aggressive solutions of 1.0 M HCl were prepared by dilution of analytical grade 37% HCl with distilled water. The concentration range of 1-methyl-4-methylsulfanyl-1H-pyrazolo[3,4-d]pyrimidine (MMPP) used was 10^{-6}M to 10^{-3}M.

2.3. Synthesis

To a solution of 1H-pyrazolo [3,4-d] pyrimidine-4-thiol (0.5 g, 3.28 mmol) dissolved in DMF (20 ml) was added iodomethane (0.43 ml, 6.62 mmol), potassium carbonate (0.93 g, 7.1 mmol) and catalytic amount of tetra-n-butylammonium bromide (0.1 g, 0.4 mmol). The mixture was stirred for 48 h and monitored by thin layer chromatography. The mixture was filtered and the solvent was removed in vacuo. The solid obtained was crystallized from ethanol to give the title compound as orange crystals (yield: 65%) El Fal et al [36-38]. The product obtained was characterized by ^{1}H NMR, ^{13}CNMR and RX.

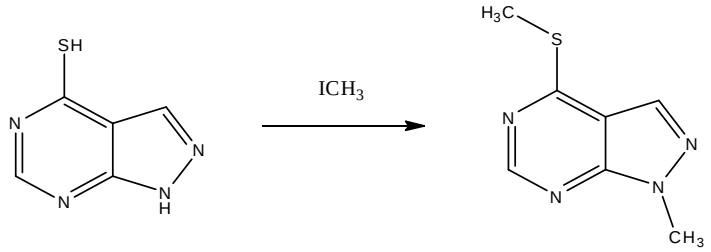

Schema 1: Alkylation of 1H-pyrazolo [3,4-d] pyrimidine-4-thiol.

The compound was characterized by N.M.R and RX. 1H-NMR (DMSO-d6) (d ppm): 2.77(s, 3H, S-CH3), 4.11 (s, 3H, N-CH3), 8.01 (s, 1H, H-3), 8.44 (s, 1H, H-6). 13C-NMR (DMSO-d6) (d ppm) : 13.3 (S-CH3), 39.4 (N-CH3), 109.8(C,C-3a), 135.08(CH, C-3), 151.06(CH, C-6), 155,5(C,C-7a), 161.03(C-S, C-4).

An X-ray crystallographic study of a single crystal of MMPP Figure 1, confirmed the structure deduced from NMR spectroscopic studies.

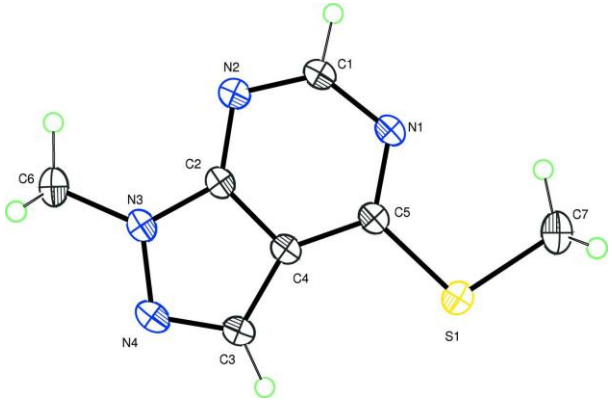

Figure 1: An ORTEP presentation of compound MMPP.

2.4. Corrosion tests

2.4.1. Electrochemical measurements

The electrochemical measurements were carried out using Volta lab (Tacussel- Radiometer PGZ 100) potentiostat and controlled by Tacussel corrosion analysis software model (Voltamaster 4) at under static condition. The corrosion cell used had three electrodes. The reference electrode was a saturated calomel electrode (SCE). A platinum electrode was used as auxiliary electrode of surface area of 1 cm^2. The working electrode was mild steel. All potentials given in this study were referred to this reference electrode. The working electrode was immersed in test solution for 30 min to a establish steady state open circuit potential (Eocp). After measuring the Eocp, the electrochemical measurements were performed. All electrochemical tests have been performed in aerated solutions at 303 K. The EIS experiments were conducted in the frequency range with high limit of 100 kHz and different low limit 0.01 Hz at open circuit potential, with 10 points per decade, at the rest potential, after 30 min of acid immersion, by applying 10 mV ac voltage peak-to-peak. Nyquist plots were made from these experiments. The impedance data were analysed and fitted with the simulation ZView 2.80, equivalent circuit software.

After ac impedance test, the potentiodynamic polarization measurements of mild steel substrate in inhibited and uninhibited solution were scanned from cathodic to the anodic direction between -800mV to -100 mV, with a scan rate of 1 mV s^{-1}. The potentiodynamic data were analysed using the polarization VoltaMaster 4 software. The linear Tafel segments of anodic and cathodic curves were extrapolated to corrosion potential to obtain corrosion current densities (I_{corr}). From the polarization curves obtained, the corrosion current (I_{corr}) was calculated by curve fitting using the equation:

$$I = I_{corr}\left[exp\left(\frac{2.3\Delta E}{\beta_a}\right) - exp\left(\frac{2.3\Delta E}{\beta_c}\right)\right] \quad (1)$$

β_a and β_c are the anodic and cathodic Tafel slopes and ΔE is $E-E_{corr}$.

The inhibition efficiency was evaluated from the measured I_{corr} values using the following relationship:

$$\eta_{Tafel}(\%) = \frac{I_{corr} - I_{corr(i)}}{I_{corr}} \times 100 \quad (2)$$

where I_{corr} and $I_{corr(i)}$ are the corrosion current densities for steel electrode in the uninhibited and inhibited solutions, respectively.

2.4.2. Computational procedures

Density Functional theory (DFT) has been recently used [39-42], to describe the interaction between the inhibitor molecule and the surface as well as the properties of these inhibitors concerning their reactivity. The molecular band gap was computed as the first vertical electronic excitation energy from the ground state using the time-dependent density functional theory (TD-DFT) approach as implemented in Gaussian 03 [43]. For these seek, some molecular descriptors, such as HOMO and LUMO energy values, frontier orbital energy gap, molecular dipole moment, were calculated using the DFT method and have been used to understand the properties and activity of the newly prepared compounds and to help in the explanation of the experimental data obtained for the corrosion process.

3. Electrochemical measurement

3.1. Potentiodynamic polarization

Polarization studies were performed to obtain knowledge about the kinetics of anodic and cathodic reactions. The potentiodynamic polarization curves for mild steel in acid solution in the absence and presence of different concentrations of MMPP are shown in Fig. 2. Electrochemical kinetic parameters, i.e., corrosion potential (E_{corr}) cathodic Tafel slopes (β_c) and corrosion current density (I_{corr}), obtained by extrapolation of the tafel lines, are presented in Table 1. As it can be seen from Fig. 2, both the cathodic and the anodic curves shift toward lower current densities, which indicate that the hydrogen ions reduction as well as the mild steel anodic dissolution is restrained in the inhibited corrosive solution. The inhibition effect is enhanced with increasing the inhibitor's concentration, this observation is indicative of the adsorption property of the inhibitor molecules on the metal surface. Specifically, cathodic polarization curves at all given inhibitor concentration display nearly parallel Tafel lines, suggesting that the existence of inhibitor does not modify the hydrogen reduction mechanism and the cathodic process is activation-controlled.

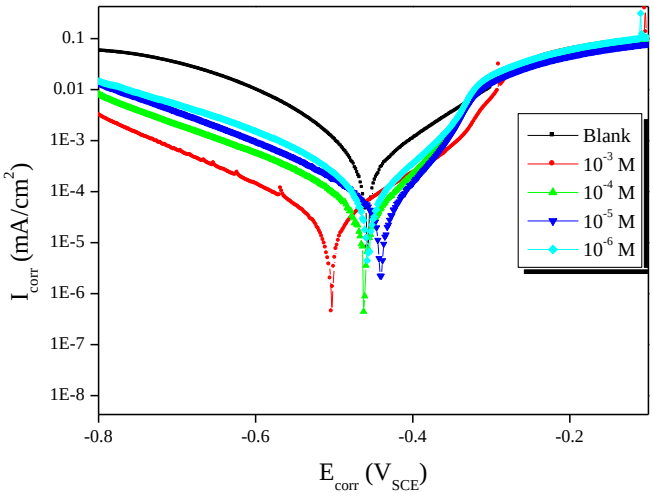

Figure 2: Polarization curves of mild steel in 1.0 M HCl containing different concentrations of MMPP.

The inhibitor acts simply by adsorbing on the metal surface and forming a protective film, which leads the decrease in the metal surface area where being attacked by H^+ ions. In the anodic region of polarization curves, the addition of MMPP decreases the current densities significantly in a wide range, and this inhibiting effect is more profound with increasing inhibitor concentration, especially at high concentration. This result also indicates that the inhibiting property is concentration independent. As the polarization potential shift toward higher over-voltage range, the anodic polarization curves show that the current density increases more remarkable with rising potential. This may be due to the occurrence of significant metal dissolution at a particular potential which gives rise to the higher desorption rate of the tested inhibitor molecule than its adsorption rate [44]. This special potential is generally described as desorption potential which is easier to be found at higher concentrations in our investigated system. In addition, it seems that the inhibitor has zero inhibitive influence on the anodic polarization curves when the potential is higher than -280 mV. This result indicates that the adsorption mode of inhibitor depends on the electrode potential.

As it is shown in Table 1, the addition of inhibitor leads to a significant decrease in the corrosion current density, and β_c values move slightly in the solution containing MMPP, showing that both the cathodic and anodic reactions are retarded through the inhibitor's adsorption on electrode surface. The values of β_c remain almost unchanged, suggesting hydrogen evolution is activation-controlled, and the addition of inhibitors does not affect the mechanism of cathodic hydrogen evolution reaction. The largest displacement in E_{corr} value is less than 85 mV, signifying that MMPP is a mixed type inhibitor [45]. The current density and the corrosion rate decrease, while the inhibition efficiency enhances with the increase of the inhibitor concentration, illustrating that a more complete and stable protective film can be formed on the metal surface at higher concentration.

Table 1: Polarization parameters and the corresponding inhibition efficiency of mild steel corrosion in 1.0 M HCl containing different concentrations of MMPP at 303 K.

C_{inh} (M)	E_{corr} (mV/SCE)	$-\beta_c$ (mV dec^{-1})	I_{corr} (µA cm^{-2})	η_{Tafel} (%)
Blank	-449	141.1	391.0	—
10^{-3}	-501	134.5	19.7	95
10^{-4}	-462	138.4	34.9	91
10^{-5}	-444	135.5	67.1	83
10^{-6}	-458	136.3	74.8	81

3.2. Electrochemical impedance spectroscopy

3.2.1. Effect of concentration inhibitor

Fig. 3 shows the Nyquist diagrams for the corrosion of steel in 1.0 M HCl in the absence and presence of various concentrations of MMPP. These diagrams have similar shape throughout all tested concentrations, indicating that almost no change in the corrosion mechanism occurs due to the inhibitor addition [46]. The diameter of the capacitive loop in the presence of inhibitor is bigger than that in the absence of inhibitor. This increase is more pronounced with increasing inhibitor concentration which indicates the adsorption of inhibitor molecules on the metal surface. As it can be seen from Fig. 3, the Nyquist plots did not yield perfect semicircles as expected from the theory of EIS. The deviation from ideal semicircle is generally attributed to the frequency dispersion as well as to the in homogeneities of surface and mass transport resistant [47]. The obtained EIS data were fitted to the electrical equivalent circuit diagram given in Fig. 4 in order to model the steel/solution interface and the parameters of circuit, electrolyte resistance (R_s), charge transfer resistance (R_{ct}) and double layer capacitance (C_{dl}) were calculated.

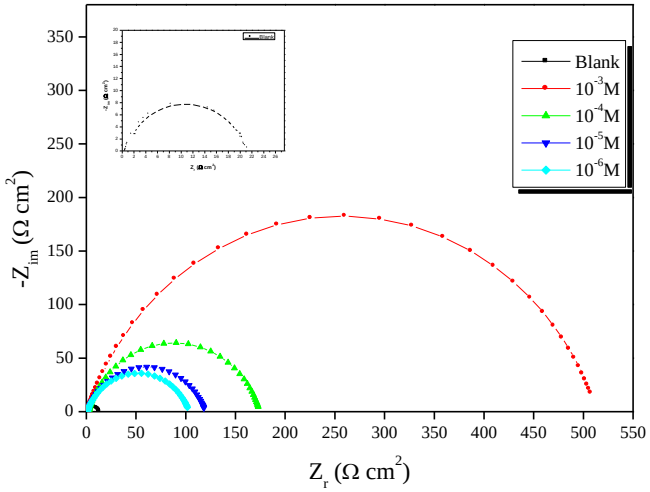

Figure 3: EIS obtained in 1.0 M HCl solution with and without various concentrations of MMPP.

The impedance function of the CPE is represented by the expression [48,49]:

$$Z_{CPE} = \frac{1}{Q(j\omega)^n} \quad (3)$$

where Q is the magnitude of the CPE, j is the imaginary number ($j^2 = -1$), ω is the angular frequency. n is the deviation parameter($-1 \leq n \leq +1$), has the meaning of a phase shift. While n = 0, the CPE represents a pure resistor, for n = -1 an inductor and for n = +1, a pure capacitor [50]. The double layer capacitance (Cdl) can be simulated via CPE from the following equation [51,52]:

$$C_{dl} = Q_{dl} \times (2\pi f_{max})^{n-1} \quad (4)$$

where f_{max} is the frequency at the maximum value of the imaginary part of the impedance spectrum. Table 2 illustrates the equivalent circuit parameters for the impedance spectra of corrosion of steel in 1.0 M HCl solution. The data indicate that increasing charge transfer resistance is associated with a decrease in the double layer capacitance. It has been reported that the adsorption of organic inhibitor on the metal surface is characterized by a decrease in C_{dl}. The decreased values of C_{dl} may be due to the replacement of water molecules at the electrode interface by organic inhibitor of lower dielectric constant through adsorption, suggests that MMPP inhibitor acts by adsorption at the metal-solution interface. The increase in values of R_{ct} and the decrease in values of C_{dl} with increasing the concentration also indicate MMPP acts as primary interface inhibitor and the charge transfer controls the corrosion of steel under the open circuit conditions [53].

The inhibition efficiency η_z(%) is calculated by R_{ct} using Eq. (5), where, R_{ct}° and R_{ct}^{i} are the charge transfer resistance in absence and in presence of inhibitor, [48], respectively:

$$\eta_z\% = \frac{R_{ct}^{i} - R_{ct}^{\circ}}{R_{ct}^{i}} \times 100 \qquad (5)$$

It is obvious that the increase in inhibitor concentration enhances R_{ct}, and consequently improves the inhibition efficiency till reaching their maximum value at 10^{-3} M (R_{ct} = 506 Ω cm^2, η_Z(%) = 96). The η(%) values obtained from the ac impedance technique are comparable and run parallel with those obtained from the potentiodynamic polarization method.

Figure 4: Equivalent circuit used for the fitting procedure of the experimental EIS data.

Table 2; EIS parameters for the corrosion of mild steel in 1.0 M HCl containing MMPP at 303 K.

C (M)	R_{ct} (Ω cm^2)	C_{dl} (μF cm^{-2})	η_z (%)
Blank	21	371	—
10^{-3} MMPP	506	48	96
10^{-4} MMPP	173	125	88
10^{-5} MMPP	120	167	83
10^{-6} MMPP	104	174	80

3.2.2. Effect of temperature

To ensure the effectiveness of MMPP under various conditions, tests were performed in 1.0 M HCl solution at different temperatures (303-333 K). The concentration of MMPP which gave the highest η_Z(%) value in 1.0 M HCl solution at 303 K (10^{-3} M) was chosen for further study.

The effect of solution temperature on the impedance spectra recorded in the studied acid solutions without and with 10^{-3} M of MMPP has been studied. In all cases, the charge transfer resistances are decreased with increasing the temperature. Nyquist plots obtained at different temperatures in 1.0 M HCl solution without and with MMPP are shown in Figs. 5 and 6, respectively.

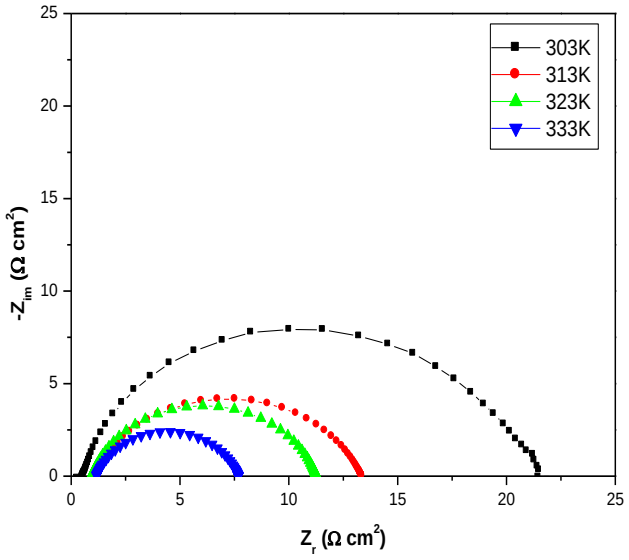

Figure 5: Nyquist plots for corrosion of steel in 1.0 M HCl at different temperature.

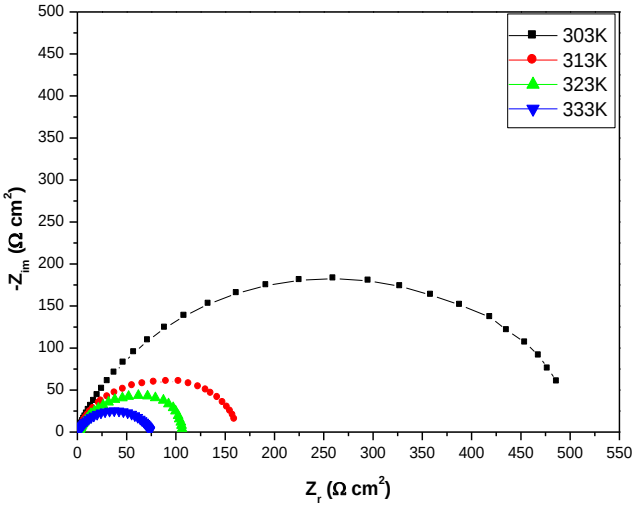

Figure 6: Nyquist plots for corrosion of steel in 1.0 M HCl + 10^{-3} MMPP at different temperatures.

These spectra reveal that although values the charge transfer resistances are decreased with increasing the temperature, these values are higher in presence of extract than in its absence. The impedance spectra obtained are quite similar to those obtained in 1.0 M HCl in the absence and presence of MMPP at different temperatures. For analysis of the impedance spectra exhibiting one capacitive loop, the equivalent circuit given in Fig. 4 was used to fit the experimental spectra.

The various corrosion parameters obtained in 1.0 M HCl solution in absence and presence of 10^{-3} M of MMPP are given in Table 3. Values of Rct obtained in presence and absence of MMPP are decreased with increasing the temperature and its values are much higher in the inhibited acidic solution which means the corrosion inhibition process by the MMPP. Values of C_{dl} obtained in 1.0 M HCl solution drastically increased indicating the high corrosion rate of steel at elevated temperatures and then remain approximately unchanged. In presence of MMPP, values of C_{dl} are slightly increased with the rise of temperature and are still lower than those obtained in the pure medium.

Table 3: EIS parameters and the corresponding inhibition efficiencies at various temperatures studied of mild steel in 1.0 M HCl containing 10^{-3} M of MMPP.

Inhibitor	Temp (K)	R_{ct} (Ω cm^2)	C_{dl} (μF cm^{-2})	η_z (%)
Blank	303	21	156	—
	313	14	176	—
	323	11	182	—
	333	7.5	197	—
MMPP	303	506	20	96
	313	160	21	91
	323	104	22	89
	333	67	35	88

Values of R_{ct} were employed to calculate values of the corrosion current density (I_{corr}) at various temperatures in absence and presence of MMPP using the following equation [54]:

$$I_{corr} = RT\left(zFR_{ct}\right)^{-1} \qquad (6)$$

where R is the universal gas constant (R = 8.314 J mol^{-1} K^{-1}), T is the absolute temperature, z is the valence of iron (z = 2), F is the Faraday constant (F = 96 485 coulomb) and R_{ct} is the charge transfer resistance.

In order to calculate activation parameters for the corrosion process, Arrhenius (7) and an alternative formulation of Arrhenius (8) were used:

$$I_{corr} = A\exp\left(-\frac{E_a}{RT}\right) \quad (7)$$

$$I_{corr} = \frac{RT}{Nh}\exp\left(\frac{\Delta S_a}{R}\right)\exp\left(\frac{\Delta H_a}{RT}\right) \quad (8)$$

where I_{corr} is the corrosion current density, K the Arrhenius preexponential constant, E_a is the activation energy for the corrosion process, h is the Plank's constant, N is the Avogadro's number, the enthalpy of activation (ΔH_a), and the entropy of activation (ΔS_a). Fig. 7 show typical plots of Ln I_{corr} vs. 1/T for the uninhibited and inhibited solutions while Fig. 8 shows a representative plot for the transition state in 1.0 M HCl solutions without and with of 10^{-3} M of MMPP. Activation parameters obtained from these graphs are given in Table 4.

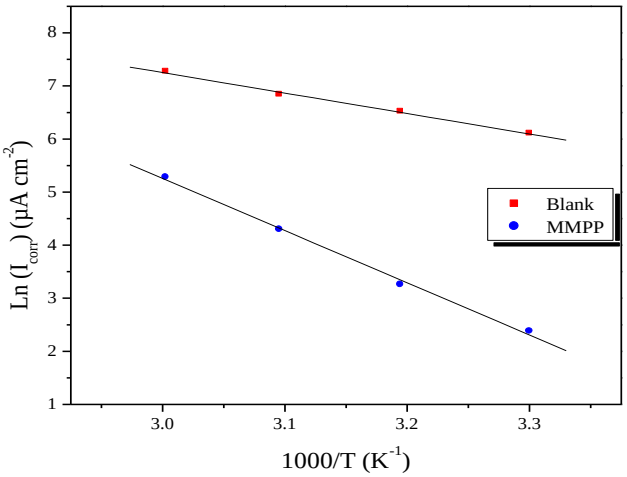

Figure 7: Arrhenius plots for mild steel corrosion rates Ln (I_{corr}) versus 1/T in 1.0 M HCl in absence and in presence of optimum concentration of MMPP.

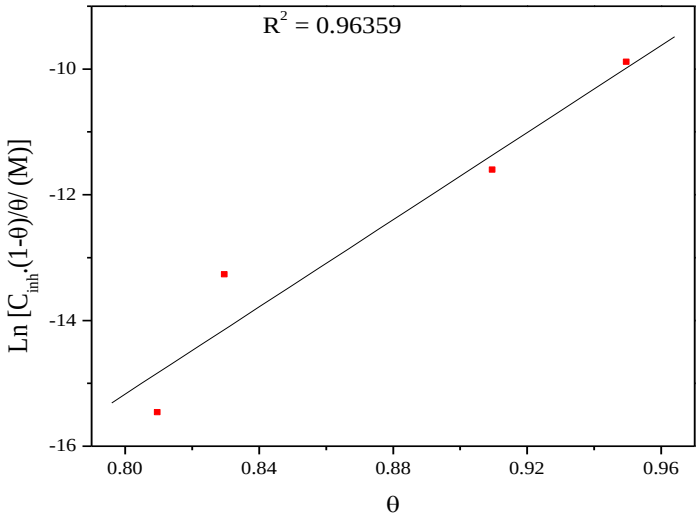

Figure 8: Transition-state plots for mild steel corrosion rates Ln (I_{corr}/T) versus 1/T in 1.0 M HCl in absence and in presence of optimum concentrations of MMPP.

Table 4: The values of activation parameters for mild steel in 1.0 M HCl in the absence and presence of optimum concentration of MMPP.

	R^2	K	E_a (kJ mol^{-1})	ΔH_a (kJ mol^{-1})	ΔS_a (J mol^{-1} K^{-1})
Blank	0.99767	1.5014×10^{9}	32.08	29.44	-97.22
MMPP	0.99840	1.2479×10^{15}	81.76	79.12	32.24

In 1.0 M HCl solution, the addition of MMPP leads to an increase in the apparent activation energy to value greater than that of the uninhibited solution. The results show that the addition of MMPP decreases metal dissolution in 1.0 M HCl medium. On the other hand, the increase in the apparent activation energy may be interpreted as physical adsorption that occurs in the first stage [55]. Szauer and Brand explained that the increase in activation energy can be attributed to an appreciable decrease in the adsorption of the inhibitor on the mild steel surface with increase in temperature. The value of E_a is larger than the analogous value of ΔHa indicating that the corrosion process must involved a gaseous reaction, simply the hydrogen evolution reaction, associated with a decrease in the total reaction volume [56].

The thermodynamic parameters (ΔH_a and ΔS_a) of the dissolution reaction of steel in 1.0 M HCl in the presence of MMPP is higher than that of in the absence of inhibitor (blank). The positive signs of the enthalpies ΔH_a reflect the endothermic nature of the steel dissolution process and mean that the dissolution of steel is difficult [57]. In the presence of MMPP, the increase of ΔS_a reveals that an increase in disordering takes place on going from reactants to the activated complex [58].

3.3. Adsorption isotherm

Adsorption isotherms are very important in understanding the mechanism of organo-electrochemical reactions [59]. In order to evaluate the adsorption process of MMPP on mild steel surface, Langmuir, Temkin and Frumkin adsorption isotherms were obtained according to the following equations:

Langmuir : $$\frac{C_{inh}}{\theta} = \frac{1}{K_{ads}} + C_{inh} \quad (9)$$

Temkin : $$\exp\left(-2a\theta\right) = bC_{inh} \quad (10)$$

Frumkin : $$\left(\frac{\theta}{1-\theta}\right)\exp\left(-2a\theta\right) = bC_{inh} \quad (11)$$

where θ is the surface coverage of the metal surface, K_{ads} the adsorption-desorption equilibrium constant, C_{inh} the inhibitor concentration and a is the lateral interaction term describing the molecular interactions in the adsorption layer and the heterogeneity of the surface. The fractional coverage values θ as a function of inhibitor concentration can be obtained from polarization as follows:

$$\theta = \frac{I_{corr} - I_{corr(i)}}{I_{corr}} \quad (12)$$

where I_{corr} and $I_{corr(i)}$ are the corrosion current densities for steel electrode in the uninhibited and inhibited solutions, respectively.

To determine which adsorption isotherm best fits the surface's coverage, the respective plots were obtained in Figs. 9-11. These curves represent adsorption isotherms that are characterized by, in a first part, a sharp rising, followed by another part, a gradual rising (less significant than in the first part), indicating formation of an adsorbed molecules layer on the mild steel surface. By far, the best fit was obtained with the Langmuir isotherm (strong correlation R_2 = 0.99999). The plots of C_{inh}/θ vs. Cinh yield a straight line (Fig. 9). This confirms that the inhibitor obeys Langmuir adsorption isotherm at 1.0 M HCl medium. It indicates that the adsorbing MMPP species occupies typical adsorption site at the metal/solution interface.

Gibbs free energy (ΔG°_{ads}) could be calculated with the following equation [60]:

$$\Delta G^{\circ}_{ads} = -RTLn(55.5K_{ads}) \quad (13)$$

Where R is gas constant and T is absolute temperature of experiment and the constant value of 55.5 is the concentration of water in solution in mol L^{-1}. In Fig. 9, the intercept on the vertical axis is the value of 1/ K_{ads}, which is 2.08958×10^{-6} M. Generally, values of ΔG°_{ads} up to -20 kJ/mol, the types of adsorption were regarded

as physisorption, the inhibition acts due to the electrostatic interactions between the charged molecules and the charged metal, while values around -40 kJ/mol or smaller are associated with chemisorption as a result of sharing or transfer of electrons from organic molecules to the metal surface to form a coordinate type of bond (chemisorption) [61]. Then according to Eq. (13), we calculated the ΔG°_{ads} = -43.06 kJ/mol. Therefore it can be concluded that the adsorption of the MMPP on the carbon steel surface is more chemical than physical [62].

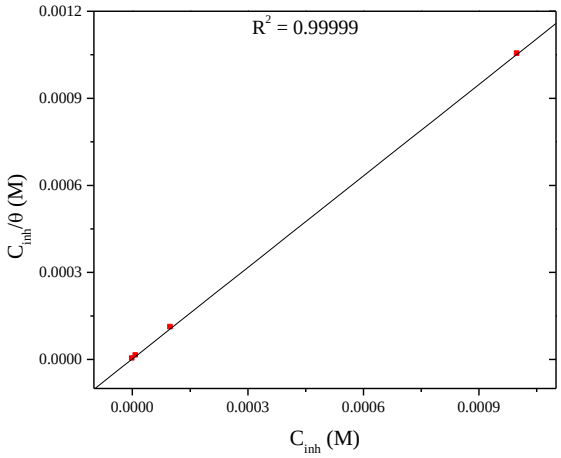

Figure 9: Langmuir adsorption plots for mild steel in 1.0 M HCl containing different concentrations of MMPP.

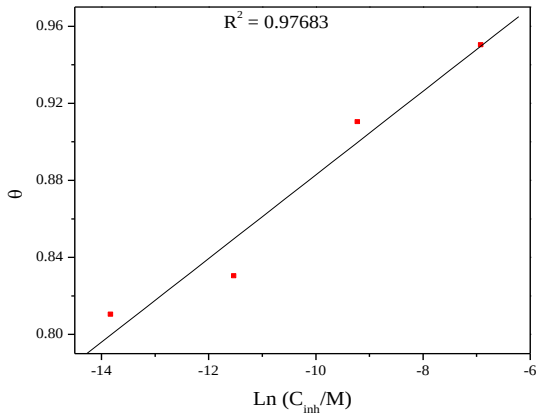

Figure 10: Temkin adsorption plots for mild steel in 1.0 M HCl containing different concentrations of MMPP.

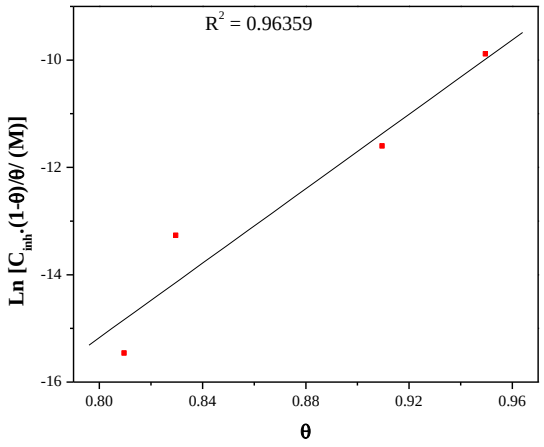

Figure 11: Frumkin adsorption plots for mild steel in 1.0 M HCl containing different concentrations of MMPP.

3.4. Quantum chemical calculations

The structure and electronic parameters were obtained by means of theoretical calculations using the computational methodologies of quantum chemistry. The optimized molecular structures and frontier molecular orbital density distribution of the studied molecule are shown in Figure 12. The calculated quantum chemical parameters such as E_{HOMO}, E_{LUMO}, $\Delta E_{LUMO-HOMO}$, dipole moments (μ) are listed in Table 5. The molecular structure of MMPP shows that the molecules seems to adsorb on steel surface by sharing of electrons of the nitrogen and sulfur atoms with iron to form coordinated bonds and π-electron interactions of the aromatic rings.

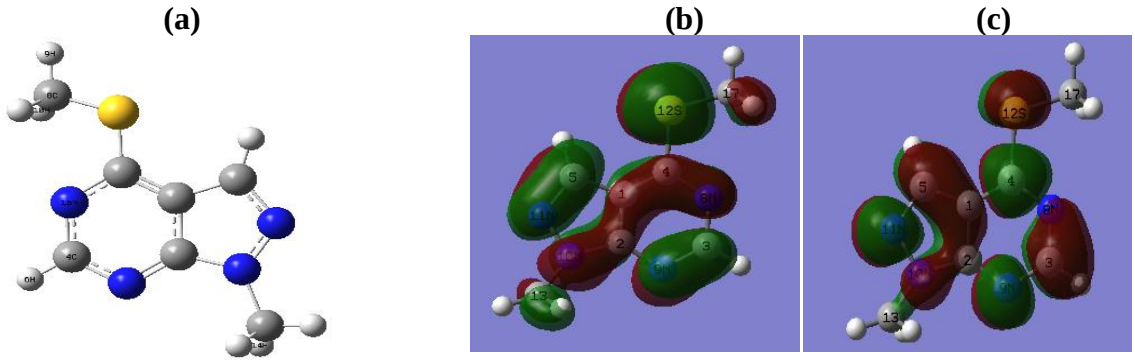

Figure 12: (a) Optimized molecular structure (b) total charge density (c) HOMO (d) LUMO molecular orbital density distribution of MMPP.

Table 5: Calculated quantum chemical parameters of MMPP.

Quantum parameters	MMPP
E_{HOMO} (eV)	-0.22553
E_{LUMO} (eV)	-0.06126
$\Delta E_{LUMO-HOMO}$	0.16427
Dipole Moment (μ)	3.9041

The value of highest occupied molecular orbital, E_{HOMO} indicates the tendency of the molecule to donate electrons to acceptor molecule with empty and low energy orbital. Therefore, the energy of the lowest unoccupied molecular orbital, E_{LUMO} indicates the tendency of the molecule to accept electrons [63]. The energy gap ΔE is an important parameter which is related to reactivity of the inhibitor molecule towards the metal surface. The interaction of inhibitor molecule to the metal surface is related to transfer of electrons from inhibitor to metal surface. Polarity of a covalent bond (Dipole moment μ) can be understood by distribution of electrons in a molecule and large value of dipole moment μ favour the adsorption of inhibitor.

Conclusion

In this study, corrosion inhibition efficiency of 1-methyl-4-methylsulfanyl-1H-pyrazolo[3,4-d]pyrimidine (MMPP) on mild steel in 1.0 M HCl was determined by electrochemical analysis and Quantum chemical calculations. In the concentration range of 10^{-6}M to 10^{-3}M, MMPP shows a good inhibition performance for mild steel in 1.0 M HCl solution. The inhibition efficiency of MMPP increases with increasing inhibition concentration and decreases with the increase of temperature in the studied temperature range. MMPP acts as a mixed-typed inhibitor which suppresses both the anodic and cathodic process by predominant chemisorption on the steel surface, and its adsorption obeys Langmuir adsorption isotherm. Electrochemical impedance spectroscopy data reveals increase in R_{ct} values, which accounted for good inhibition efficiency. Quantum chemical studies also support the experimental studies.

Acknowledgments

The authors are pleased to recognize Professors Abdelfettah Zerzouf and Nour-Eddin Essafi Laboratory of Physico-Chemistry of Inorganic and Organic Materials (LPCMIO), ENS, Rabat, Morocco for his kind and For chemical synthesis characterization.

References

1. Babu B.R., Thangavel K., *Anti-Corros. Method Mater*. 52 (2005) 219.
2. Fouda A.S., Mostafa H.A., Heakal F.E., Elewady G.Y., *Corros. Sci*. 47 (2005) 1988.
3. Yurchenko R., Pogrebova L., Pilipenko T., Shubina T., *Russ. J. Appl. Chem*. 79 (2006) 1100.
4. Zarrouk, A., Zarrok, H., Salghi, R., Hammouti, B., Bentiss, F.,Touir, R., Bouachrine, M., *J. Mater. Environ. Sci*. 4 (2013) 177.
5. Belayachi M., Serrar H., Zarrok H., El Assyry A., Zarrouk A., Oudda H., Boukhris S., Hammouti B., Ebenso Eno E., Geunbour A., *Int. J. Electrochem. Sci*. 10 (2015) 3010.
6. Zarrok H., Zarrouk A., Salghi R., Ramli Y., Hammouti B., Assouag M., Essassi E. M., Oudda H., Taleb M., *J. Chem. Pharm. Res*. 4 (2012) 5048.
7. Ghazoui A., Benchat N., El-Hajjaji F., Taleb M., Rais Z., Saddik R., Elaatiaoui A., Hammouti B., *Journal of Alloys and Compounds*, 693 (2017) 510-517
8. Ghazoui A., Saddik R., Benchat N., Guenbour M., Hammouti B., Al-Deyab S.S., Zarrouk A., *Int. J. Electrochem. Sci*. 7 (2012) 7080.
9. Ghazoui A., Zarrouk A. , Bencaht N. , Salghi R. , Assouag M. , El Hezzat M. , Guenbour A. , Hammouti B. , *J. Chem. Pharm. Res*. 6 (2014) 704.
10. Zarrok H., Zarrouk A. , Salghi R. , Ebn Touhami M., Oudda H. , Hammouti B., Touir R. , Bentiss F. , Al-Deyab S.S. , *Int. J. Electrochem. Sci*. 8 (2013) 6014.
11. Tayebi H., Bourazmi H., Himmi B., El Assyry A., Ramli Y., Zarrouk A., Geunbour A., Hammouti B., Ebenso Eno E., *Der Pharm. Lett*. 6(6) (2014) 20.
12. Tayebi H., Bourazmi H., Himmi B., El Assyry A., Ramli Y., Zarrouk A., Geunbour A., Hammouti B., *Der Pharm. Chem*. 6(5) (2014) 220.
13. ELaoufir Y., Bourazmi H., Serrar H., Zarrok H., Zarrouk A., Hammouti B., Guenbour A., Boukhriss S., Oudda H., *Der Pharm. Lett*. 6(4) (2014) 526.
14. Zarrouk A., Hammouti B. , Dafali A. , Bentiss F., *Ind. Eng. Chem. Res*. 52 (2013) 2560.
15. Zarrouk A., Hammouti B., Zarrok H., Bouachrine M., Khaled K.F., Al-Deyab S.S., *Int. J. Electrochem. Sci.* 6 (2012) 89.
16. Zarrok H., Al Mamari K., Zarrouk A., Salghi R., Hammouti B., Al-Deyab S. S., Essassi E. M., Bentiss F., Oudda H., *Int. J. Electrochem. Sci*. 7 (2012) 10338.
17. Zarrok H., Oudda H., El Midaoui A., Zarrouk A., Hammouti B., Ebn Touhami M., Attayibat A., Radi S., Touzani R., *Res. Chem. Intermed*. 38 (2012) 2051.
18. Zarrok H., Zarrouk A., Salghi R., Oudda H., Hammouti B., Assouag M., Taleb M., Ebn Touhami M., Bouachrine M., Boukhris S., *J. Chem. Pharm. Res*. 4 (2012) 5056.
19. Zarrouk A., Zarrok H., Salghi R., Touir R., Hammouti B., Benchat N., Afrine L.L., Hannache H., El Hezzat M., Bouachrine M. , *J. Chem. Pharm. Res*. 5 (2013) 1482.
20. Zarrok H., Zarrouk A., Salghi R., Assouag M., Hammouti B., Oudda H., Boukhris S., Al Deyab S.S., Warad I., *Der Pharm. Lett*. 5 (2013) 43.
21. Ben Hmamou D., Aouad M.R., Salghi R., Zarrouk A., Assouag M., Benali O., Messali M., Zarrok H., Hammouti B., *J. Chem. Pharm. Res*. 4 (2012) 3498.
22. Belayachi M., Serrar H., El Assyry A., Oudda H., Boukhris S., Ebn Touhami M., Zarrouk A., Hammouti B., Ebenso Eno E., El Midaoui A., *Int. J. Electrochem. Sci*. 10 (2015) 3038.
23. El Hezzat M., Assouag M., Zarrok H., Benzekri Z., El Assyry A., Boukhris S., Souizi A., Galai M., Touir R., Ebn Touhami M., Oudda H., Zarrouk A., *Der Pharm. Chem.* 7(10) (2015) 77
24. EL Arouji S., Alaoui Ismaili K., Zerrouki A., El Kadiri S., Rais Z., Filali Baba M., Taleb M., Emran Khadijah M., Zarrouk A., Aouniti A., Hammouti B., *Der Pharm. Chem.* 7(10) (2015) 67.
25. ELouadi Y., Abrigach F., Bouyanzer A., Touzani R., Riant O., ElMahi B., El Assyry A., Radi S., Zarrouk A., Hammouti B., *Der Pharm. Chem*. 7(8) (2015) 265.
26. Benhiba F., Zarrok H., Elmidaoui A., El Hezzat M., Touir R., Guenbour A., Zarrouk A., Boukhris S., Oudda H., *J. Mater. Environ. Sci*. 6(8) (2015) 2301.
27. Belayachi M., Zarrok H., Larouj M., Zarrouk A., Bourazmi H., Guenbour A., Hammouti B., Boukhriss S., Oudda H., *Phys. Chem. News* 74 (2014) 85.
28. Zarrok H., Al-Deyab S.S., Zarrouk A., Salghi R., Hammouti B., Oudda H., Bouachrine M., Bentiss F., *Int. J. Electrochem. Sci*. 7 (2012) 4047.
29. Zarrok H., Zarrouk A., Salghi R., Oudda H., Hammouti B., Ebn Touhami M., Bouachrine M., Pucci O.H., *Port. Electrochim. Acta* 30 (2012) 405.
30. Afrine L., Zarrouk A., Zarrok H., Salghi R., Touir R., Hammouti B., Oudda H., Assouag M., Hannache H., El Harti M., Bouachrine M., *J. Chem. Pharm. Res*. 5 (2013) 1474.
31. Zarrouk A., El Ouali I., Bouachrine M., Hammouti B., Ramli Y., Essassi E.M., Warad I., Aouniti A., Salghi R., *Res. Chem. Intermed*. 39 (2013) 1125.
32. Zarrouk A., Hammouti B., Zarrok H., Salghi R., Bouachrine M., Bentiss F., Al-Deyab S.S., *Res. Chem. Intermed*. 38 (**2012**) 2327.

33. Zarrouk A., Hammouti B., Zarrok H., Al-Deyab S.S., Warad I., *Res. Chem. Intermed*. 38 (2012) 165.
34. Jafari H., Danaee I., Eskandari H., RashvandAvei M., *J. Environ. Sci. Health, Part A* 48 (2013) 1628.
35. Danaee I., Gholami M., RashvandAvei M., Maddahy M.H., *J. Ind. Eng. Chem*. 2014.doi:10.1016/j.jiec.2014.11.018.
36. El Fal M., Ramli Y., Essassi E.M., Saadi M., El Ammari L., *Acta Cryst. E70* (2014) o128.
37. El Fal M., Ramli Y., Essassi E.M., Saadi M., El Ammari L., *Acta Cryst. E71* (2015) o95
38. El Fal M., Ramli Y., Zerzouf A., Talbaoui A., Bakri Y., Essassi E.M., *Journal of Chemistry*, 2015, Article ID 982404, 6 pages , http://dx.doi.org/10.1155/2015/982404
39. Ma H., Chen S., Liu Z., Sun Y., *J. Mol. Struct. (THEOCHEM).* 774 (1-3) (2006) 19.
40. Henríquez-Román J.H., Padilla-Campos L., Páez M.A., Zagal J.H., María Rubio A., Rangel C.M., Costamagna J., Cárdenas-Jirón G., *J. Mol. Struct. (THEOCHEM).* 757 (1-3) (2005) 1.
41. Rodrguez-Valdez L.M., Martnez-Villafane A., Glossman-Mitnik D., *J. Mol. Struct. (THEOCHEM).* 713 (2005) 65.
42. Feng Y., Chen S., Guo W., Zhang Y., Liu G., *J. Electroanal. Chem*. 602 (1) (2007) 115.
43. M.J. Frisch, G.W Trucks, H.B. Schlegel, G.E. Scuseria, M.A. Robb, J.R. Cheeseman, Jr. J.A. Montgomery, T. Vreven, K.N. Kudin, J.C. Burant, J. M. Millam, S.S. Iyengar, J. Tomasi, V. Barone, B. Mennucci, M. Cossi, G. Scalmani, N. Rega, G.A. Petersson, H. Nakatsuji, M. Hada, M. Ehara, K. Toyota, R. Fukuda, J. Hasegawa, M. Ishida, T. Nakajima, Y. Honda, O. Kitao, H. Nakai, M. Klene, X. Li, J.E. Knox, H. P. Hratchian, J. B.Cross, V. Bakken, C. Adamo, J. Jaramillo, R. Gomperts, R.E. Stratman, O. Yazyev, A.J. Austin, R. Cammi, C. Pomelli, J.W. Ochterski, P.Y. Ayala, K. Morokuma, G.A. Voth, P. Salvador, J.J. Dannenberg, V.G. Zakrzewski, S. Dapprich, A.D. Daniels, M.C. Strain, O. Farkas, D.K. Malick, A.D. Rabuck, K. Raghavachari, J.B. Foresman, J.V. Ortiz, Q. Cui, A.G. Baboul, S. Clifford, J. Cioslowski, B.B. Stefanov, G.Liu, A. Liashenko, P. Piskorz, I. Komaromi, R.L. Martin, D.J. Fox, T. Keith, M.A. Al-Laham, C.Y. Peng, A. Nanayakkara, M. Challacombe, P.M.W. . Gill, B. Johnson, W. Chen, M.W. Wong, C. Gonzalez, J.A. Pople, Gaussian 03, Revision E.01, Gaussian, Inc., Wallingford CT (2004).
44. Kamal C., M.G. Sethuraman, *Arab. J. Chem*. 5 (2012) 155.
45. Ansari K.R., Quraishi M.A., *J. Ind. Eng. Chem*. 20 (2014) 2819.
46. Labjar N., Lebrini M., Bentiss F., Chihib N.E., El Hajjaji S., Jama C., *Mater. Chem. Phys*. 119 (2010) 330.
47. Danaee I., Noori S., *Int. J. Hydrogen Energy* 36 (2011) 12102.
48. Xu B., Yang W., Liu Y., Yin X., Gong W., Chen Y., *Corros. Sci*. 78 (2014) 260.
49. Li X., Xie X., Deng S., Du G., *Corros. Sci*. 87 (2014) 27.
50. Hosseini M., Mertens S.F.L., Ghorbani M., Arshadi M.R., *Mater. Chem. Phys*. 78 (2003) 800.
51. Hsu C.S., Mansfeld F., *Corrosion* 57 (2001) 747.
52. Qu Q., Jiang S.A., Bai W., Li L., *Electrochim. Acta* 52 (2007) 6811.
53. Hoseinzadeh A.R., Danaee I., Maddahy M.H., *Z. Phys. Chem.* 227 (2013) 403.
54. Tayebi H., Himmi B., Ramli Y., Zarrouk A., Geunbour A., Bellaouchou A., Zarrok H., Boudalia M., El Assyry A., *Res. J. Pharm. Biol. Chem. Sci.* 6(4) (2015) 1861.
55. Martinez S., Stern I., *Appl. Surf. Sci*. 199 (2002) 83.
56. Noor E.A., *Int. J. Electrochem*. Sci. 2 (2007) 996.
57. Guan N.M., Xueming L., Fei L., *Mater. Chem. Phys*. 86 (2004) 59.
58. Khamis E., Hosney A., El-Khodary S., *Afinidad* 52 (1995) 95.
59. Cardoso S.P., Reis F.A., Massapust F.C., Costa J.F., Tebaldi L.S., Araujo L.F.L., Silva M.V.A., Oliveira T.S., Gomes J.A.C.P., Hollauer E., *Quim. Nova* 28 (2005) 756-760.
60. Dabrowski A., *Adv. Colloid Interface Sci*. 93 (2001) 135.
61. Szklarskasmialowska Z., Mankowski J., *Corros. Sci*. 18 (1978) 953.
62. Mallaiyaa K., Subramaniama R., Srikandana S.S., Gowria S., Rajasekaranb N., Selvaraj A., *Electrochim. Acta* 56 (2011) 3857.
63. Ahamad I., Prasad R., Quraishi M.A., *J. Solid State Electrochem*. 14 (2010) 2095.

(2017) ; http://www.jmaterenvironsci.com/

.